DTU Library

Thermal conductivity of sandstones from Biot's coefficient

Orlander, Tobias; Adamopoulou, Eirini; Jerver Asmussen, Janus; Marczyski, Adam Andrzej; Milsch, Harald; Pasquinelli, Lisa; Fabricius, Ida Lykke

[Link back to DTU Orbit](#)

Thermal conductivity of sandstones from Biot's coefficient

Tobias Orlander[1], Eirini Adamopoulou[1], Janus Jerver Asmussen[1], Adam Andrzej Marczyński[1], Harald Milsch[2], Lisa Pasquinelli[1], and Ida Lykke Fabricius[1]

ABSTRACT

Thermal conductivity of rocks is typically measured on core samples and cannot be directly measured from logs. We have developed a method to estimate thermal conductivity from logging data, where the key parameter is rock elasticity. This will be relevant for the subsurface industry. Present models for thermal conductivity are typically based primarily on porosity and are limited by inherent constraints and inadequate characterization of the rock texture and can therefore be inaccurate. Provided known or estimated mineralogy, we have developed a theoretical model for prediction of thermal conductivity with application to sandstones. Input parameters are derived from standard logging campaigns through conventional log interpretation. The model is formulated from a simplified rock cube enclosed in a unit volume, where a 1D heat flow passes through constituents in three parallel heat paths: solid, fluid, and solid-fluid in series. The cross section of each path perpendicular to the heat flow represents the rock texture: (1) The cross section with heat transfer through the solid alone is limited by grain contacts, and it is equal to the area governing the material stiffness and quantified through Biot's coefficient. (2) The cross section with heat transfer through the fluid alone is equal to the area governing fluid flow in the same direction and quantified by a factor analogous to Kozeny's factor for permeability. (3) The residual cross section involves the residual constituents in the solid-fluid heat path. By using laboratory data for outcrop sandstones and well-log data from a Triassic sandstone formation in Denmark, we compared measured thermal conductivity with our model predictions as well as to the more conventional porosity-based geometric mean. For outcrop material, we find good agreement with model predictions from our work and with the geometric mean, whereas when using well-log data, our model predictions indicate better agreement.

INTRODUCTION

Thermal conductivity λ is a key parameter in subsurface applications such as geothermal plants where variations in thermal conductivity can be essential for planning and decision making. Core materials available for laboratory measurement are, however, often limited and thermal conductivities are therefore mostly estimated from empirical relations or from theoretical models based on contributions from constituents and related to the rock texture. Following the inherent constraints of purely empirical relations, such relations should be applied with great caution. However, because tools developed for in situ measurements of thermal conductivity (e.g., Freifeld et al., 2008; Moscoso Lembcke et al., 2016) are not yet part of standard logging campaigns, prediction from other downhole parameters is still required. Published work on logging-based empirical predictions includes Hartmann et al. (2005) and Fuchs and Förster (2014), where the latter do an extensive review of the previous work.

The published research on modeling thermal conductivity with application to powders, soils, as well as to porous rocks is comprehensive. Abdulagatova et al. (2009) list a large number of widely used theoretical (and empirical) models for λ. In general, the theoretical models use porosity ϕ to quantify volume of solid and fluid, and it is well-established that porosity is one of the key parameters classifying porous rocks for theoretical modeling. Further, provided that the constituent thermal conductivity is known, porosity also governs the physical maximum and minimum bounds of λ by arranging the constituents in purely serial or parallel heat paths with

relation to the direction of heat transfer. The physical bounds are denoted as Wiener (1904) bounds and are illustrated by Tong et al. (2009), but for sandstones, these bounds are generally too wide because only a bare minimum of the rock texture is captured solely through porosity. Although without physical meaning, the geometric mean is similarly porosity based but in general is closer to the measured data (e.g., Woodside and Messmer, 1961a, 1961b; Sass et al., 1971; Brigaud and Vasseur, 1989; Troschke and Burkhardt, 1998) and hence is regarded a good approximation. The geometric mean is also used as a mixing law for computation of an overall solid thermal conductivity when more than one solid constituent is taken into account (e.g., Fuchs and Förster, 2014). Using porosity and constituent thermal conductivity, the Hashin-Shtrikman formulation for isotropic and homogeneous mixtures (Hashin and Shtrikman, 1962) provides narrower bounds for sandstones compared with the Wiener bounds (Zimmerman, 1989), but it still only captures a little of the rock texture. Formulations of the geometric mean, Wiener bounds, and Hashin-Shtrikman bounds are found in Appendix A.

With respect to thermal conductivity, describing the rock texture solely through volume fractions is incomplete and, hence, methods for prediction of thermal conductivity accounting for the effects related to the texture of constituents are the subject of several studies including quantification of pore geometry (e.g., Huang, 1971), grain size (e.g., Midttomme and Roaldset, 1998), and grain shape (e.g., Revil, 2000). Adding information on the geometry of pores and solids improves the description of the rock texture. However, because the sizes of pores and solids are typically smaller than a representative volume, emphasis should be on describing the cross sections between single pores and single solids, respectively. Relating physical properties such as electrical resistivity (e.g., Revil, 2000) and elastic wave velocity (e.g., Horai and Simmons, 1969; Zamora et al., 1993; Kazatchenko et al., 2006) to thermal conductivity indirectly relates the cross sections between single pores and single solids, respectively. Because the thermal conductivity of the solid constituents found in most sandstones is typically several orders of magnitude larger than that of the saturating fluid, which for most practical applications is water, the cross section governing heat transfer is presumably that of the solid and this should hence be quantified. In general, the cross section governing solid heat transfer

is evaluated as particle to particle contacts, and this has mostly been addressed through geometric simplification of the solid rock texture within a representative volume and hence not by a measurable parameter (e.g., Deissler and Eian, 1952; Kunii and Smith, 1959; Woodside and Messmer, 1961b; Batchelor and O'Brien, 1977; Hadley, 1986; Hsu et al., 1994). Other studies are based on the concept of sedimentary rocks as a continuous but porous and/or cracked mineral (e.g., Gegenhuber and Schoen, 2012; Pimienta et al., 2014). This leads to a general concept of solid particle contacts only being accessible through mathematical modeling and not through measurements.

We follow other studies (e.g., Woodside and Messmer, 1961a; Sass et al., 1971; Huang, 1971; Tarnawski and Leong, 2012) suggesting modeling of 1D heat transfer through simplification of the rock structure in three parallel heat-transfer paths: solid, fluid, and solid-fluid in series. In the proposed model, we constrain the three heat paths in a unit volume and we determine the cross sections governing all three heat paths to capture the rock texture and its implications on thermal conductivity. In its simplest form, the model uses a minimum number of input parameters to describe the modeled rock, hence posing the maximum simplification, but this provides extensions to include a mixed mineralogy for the case in which detailed mineralogy is known.

We introduce Biot's coefficient (Biot, 1941) derived from mineralogy, bulk density, and elastic wave velocities as a measure of the solid heat transfer cross section, so we follow the conceptual idea of relating material stiffness to thermal conductivity (Horai and Simmons, 1969; Zamora et al., 1993; Kazatchenko et al., 2006; Gegenhuber and Schoen, 2012; Pimienta et al., 2014). As a measure of the cross section governing heat transfer through the pore space, we introduce a geometric factor modeled from porosity according to Mortensen et al. (1998), quantifying the proportion of the pore space that is open for fluid flow in a given direction and we assumed it to be identical to the pore space open for heat transfer. Residuals of respectively solid and pore volumes are arranged in series, which constitutes a third path of heat transfer. Then, we proceed to model thermal conductivity for dry and water-saturated sandstones using laboratory and logging data.

THEORY

Cross sections governing heat transfer

We envisage sandstones as single grains cemented together constituting a porous frame (Figure 1), and we associate solid heat transfer with rock texture through mechanical stiffness and we propose solid heat transfer cross sections equal to solid stiffness cross sections.

In the concept of effective stress and provided a drained case, Biot's coefficient α quantifies the amount of fluid pressure P, which counteracts an external stress σ and reduces resulting elastic compaction. As illustrated by Fabricius (2010) and in Figure 1, we interpret the residual of α as a quantification of the grain-to-grain contact area perpendicular to a given direction. The relation between α and the grain contact areas is discussed by Gommesen et al. (2007) and Alam et al. (2012) establishing that quantifying Biot's coefficient directly provides quantification of the grain-to-grain contact area equal to $(1 - \alpha)$.

Provided knowledge of the mineral bulk modulus $K_{\min}$, Biot's coefficient is defined as
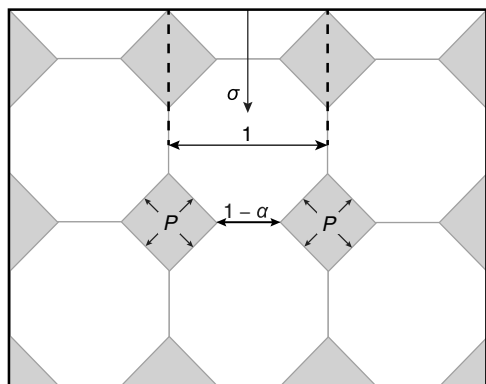

Figure 1. Conceptual sketch of a porous sedimentary rock with saturating fluid (gray) and sediment particles (white) connected by contact cement (after Fabricius, 2010). The effective stress is $\sigma' = \sigma - \alpha P$ because the pore pressure is diminished by α because it only acts on a part of the cross-sectional area.

$$\alpha = 1 - K_{\text{dra}}/K_{\min}, \tag{1}$$

where K_{dra} is the drained bulk modulus, i.e., the frame bulk modulus K_{frame}. The term K_{dra} is typically determined from compressional and shear moduli of rocks in the dry state as $K_{\text{frame}} = K_{\text{dry}} = M_{\text{dry}} - 4/3G_{\text{dry}}$, where $M_{\text{dry}} = \rho_{\text{dry}}V_{\text{P,dry}}^2$ and $G_{\text{dry}} = \rho_{\text{dry}}V_{\text{S,dry}}^2$ are compressional and shear moduli and ρ_{dry}, $V_{\text{P,dry}}$, and $V_{\text{S,dry}}$ are the dry density, dry compressional, and dry S-wave velocities, respectively. Alternatively, K_{dry} and M_{dry} can be approximated through fluid substitution of data obtained for rocks in the saturated state by, e.g., Gassmann (1951) for K_{dry} and the formulation by Mavko et al. (2009) for M_{dry}. In many cases, S-wave velocities are not available or are considered unreliable and, as a consequence, estimations of Biot's coefficient are often limited to an approximated value δ, based on compressional moduli as

$$\delta = 1 - M_{\text{dry}}/M_{\min}, \tag{2}$$

where $M_{\min}$ is the compressional mineral modulus.

We approach quantification of the cross sections of the pore space open for heat transfer through permeability and Kozeny's (1927) equation, which is formulated as

$$k = c\frac{\phi^3}{S_b}, \tag{3}$$

where k is the permeability, ϕ is the porosity, S_b is the specific surface with respect to the bulk volume, and c is the Kozeny's factor accounting for effects of shielded pore space and heterogeneous distributions of specific surface.

Kozeny's model of a porous medium uses parallel circular tubes in one direction and is in line with Poiseuille's law. By assuming the pore space as 3D orthogonal interpenetrating circular tubes, Mortensen et al. (1998) apply Poiseuille's law to derive the porosity open to flow in only one direction and derive an expression for Kozeny's factor assuming a homogeneous distribution of specific surface, hence, only accounting for shielding effects obstructing fluid flow. The expression by Mortensen et al. (1998) is

$$c_M = \left\{ 4\cos\left[\frac{1}{3}\arccos\left(\phi\frac{64}{\pi^3} - 1\right) + \frac{4\pi}{3}\right] + 4 \right\}^{-1}, \tag{4}$$

where ϕ is the porosity. Because the expression by Mortensen et al. (1998) has a different physical meaning than Kozeny's factor, it is denoted as c_M. Because the proposed model does not include effects of a specific surface, we introduce $c_M\phi$ as a quantification of the cross section governing heat transfer solely through the pore space.

A model of thermal conductivity

For modeling thermal conductivity in sandstones, we establish, within a unit volume, cross sections of (1) solid heat transfer, (2) heat transfer through the pore space, and (3) heat transfer through the residual of constituents from (1) and (2). Combined with constituent volumes, (1–3) constitute the quantitative minimum of descriptors for a representative elementary volume of a sandstone. We propose the conceptual simplification of (1–3) for a sandstone illustrated in Figure 2a. In addition, we acknowledge that for most of the sandstones, the solid consists of several minerals. However, as illustrated in Figure 2a, only one solid is

assumed to be load bearing. Hence, we introduce (4) as V_{sus} defined as the solid nonload-bearing fraction of the total solid volume and assume (4) to be part of (3), which should be modeled as a serial connection. Assuming a 1D and purely conductive heat flow, so that the presumably minor contributions from convection and radiation are neglected, we relate (1–4) to the bulk volume and we distribute all in three parallel heat paths and within the boundaries of a unit cell (Figure 2b). In line with the previous section, we propose $(1 - \alpha)$ and $c_M\phi$ as quantification of the solid heat transfer cross section, respectively, the pore space heat transfer cross section (with ϕ and $(1 - \phi)$ as the total pore volume and solid volume, respectively) and we derive $(\alpha - \phi)$ and $(1 - c_M)\phi$ as residual volumes of the solid and pore space, respectively. The residual load-bearing solid is derived as $(\alpha - \phi - V_{\text{sus}})$ and is arranged in series with V_{sus} and the residual pore space (Figure 2a).

From the proposed distribution (Figure 2b) and by assuming a constant thermal conductivity of each constituent, we derive λ from thermal conductivity in the three parallel heat paths by formulating the thermal resistance R of the paths constituting a total thermal resistance R_{tot} as

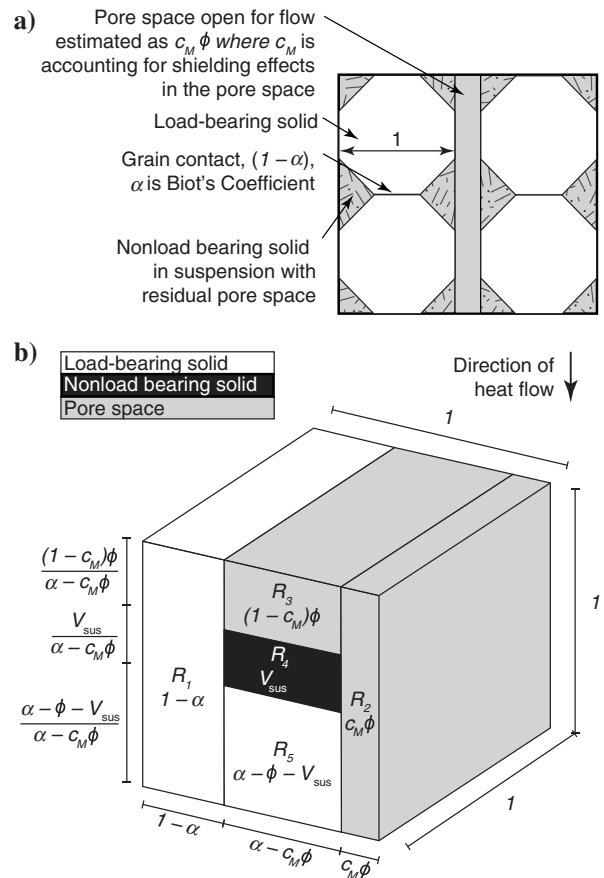$$\frac{1}{R_{\text{tot}}} = \frac{1}{R_1} + \frac{1}{R_2} + \frac{1}{R_3 + R_4 + R_5}, \tag{5}$$

Figure 2. (a) Conceptual illustration of a sandstone. (b) Partitioned rock unit volume showing distribution of the load-bearing solid, the nonload-bearing solid, the connected pore space, and the residual pore space. The figure shows the length scale and volumes of the constituents.

where R_1, R_2, R_3, R_4, and R_5 are

$$R_1 = \frac{1}{(1-\alpha)\lambda_{\mathrm{lbs}}}, \quad R_2 = \frac{1}{c_M \phi \lambda_{\mathrm{f}}},$$

$$R_3 = \frac{(1-c_M)\phi}{(\alpha - c_M \phi)^2 \lambda_f}, \quad R_4 = \frac{V_{\mathrm{sus}}}{(\alpha - c_M \phi)^2 \lambda_{\mathrm{sus}}},$$

$$R_5 = \frac{\alpha - \phi - V_{\mathrm{sus}}}{(\alpha - c_M \phi)^2 \lambda_{\mathrm{lbs}}}, \tag{6}$$

and λ_{lbs}, λ_{sus}, λ_{f} are the thermal conductivities of the load-bearing solid, the suspended nonload-bearing solid, and the saturating liquid or gaseous fluid, respectively. For a unit volume, R_{tot} is equal to $1/\lambda$, where λ is the effective thermal conductivity. Solving R_{tot} for λ equals

a)

b)

$$\lambda = (1-\alpha)\lambda_{\mathrm{lbs}} + c_M \phi \lambda_f$$

$$+ (\alpha - c_M \phi)^2 \left(\frac{(1-c_M)\phi}{\lambda_f} + \frac{V_{\mathrm{sus}}}{\lambda_{\mathrm{sus}}} + \frac{\alpha - \phi - V_{\mathrm{sus}}}{\lambda_{\mathrm{lbs}}} \right)^{-1},$$

$$(\alpha - \phi - V_{\mathrm{sus}}) \geq 0. \tag{7}$$

When two or more solids are suspended, V_{sus} and λ_{sus} must be in accordance with

$$V_{\mathrm{sus}} = \sum_{i=1}^{n} V_{\mathrm{sol},i} \quad \text{and} \quad \lambda_{\mathrm{sus}} = \sum_{i=1}^{n} \lambda_{\mathrm{sol},i}, \tag{8}$$

where V_{sol}, λ_{sol}, n, and i are the solid volume, thermal conductivity of suspended solid, the total number of nonload-bearing solids, and the ith solid, respectively.
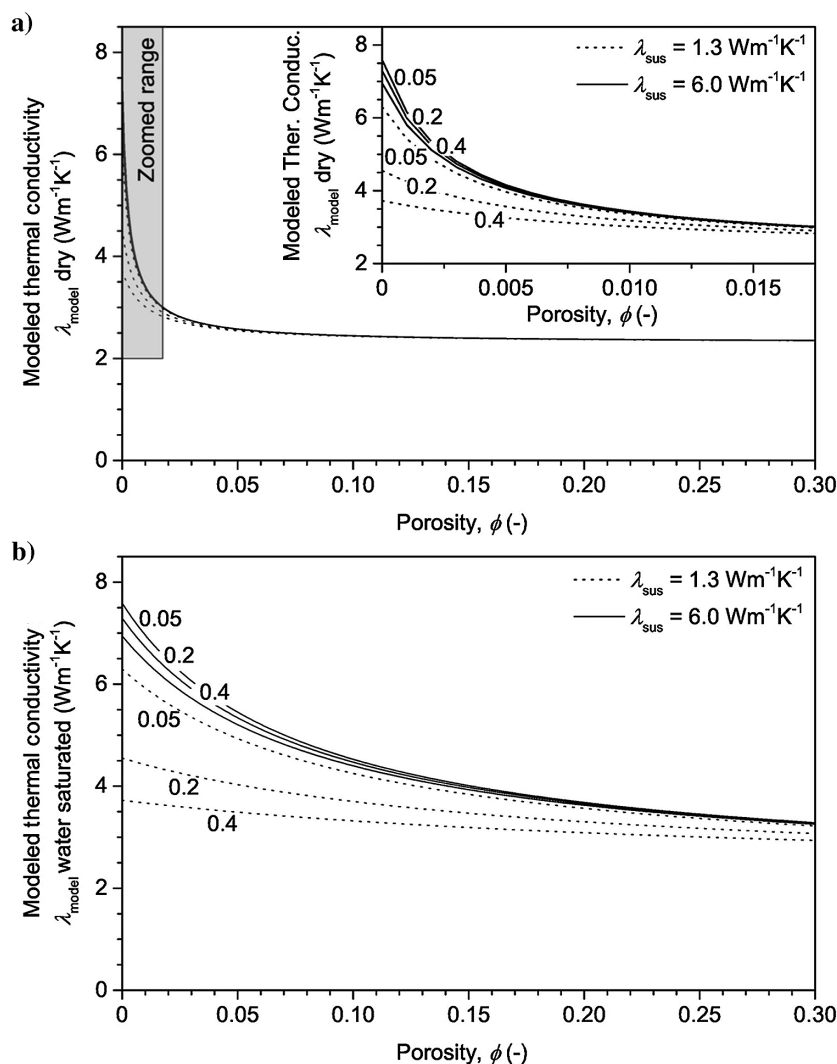
Figure 3 shows an example of model predictions from equation 7 illustrating curves for λ_{sus} equal to 1.3 and 6 Wm^{-1} K^{-1}, V_{sus} corresponding to 0.05, 0.2, 0.4, and $\lambda_{\mathrm{lbs}} = 7.7$ Wm^{-1} K^{-1}. No significant changes in model predictions are observed for changes in V_{sus} and λ_{sus} in the dry state (Figure 3a) illustrating λ_{lbs} and $(1 - \alpha)$ as the dominating contribution to λ. Significant changes in model prediction are observed in the saturated state for $V_{\mathrm{sus}} > 0.05$ and $\lambda_{\mathrm{sus}} = 1.3$ Wm^{-1} K^{-1} (Figure 3b), illustrating a significant influence of the thermal conductivity of the saturating fluid on λ, especially with the increasing volume of suspended solids with low thermal conductivity.

MATERIALS AND METHODS

We used two sets of data for validation of the proposed model (1) from laboratory measurements on outcrop sandstones and (2) downhole data from a logging campaign and corresponding core material.

Outcrop material

The studied outcrop sandstones originate from (1) Fontainebleau, France, (2) Castlegate, USA, (3) Bentheim, Germany, (4) Obernkirchen, Germany, and (5) Berea, USA, and were selected, such that a reasonable range of porosity and stiffness are represented. The bulk mineralogical composition as derived from X-ray diffraction (XRD) analysis conducted on side trims shows the dominance of quartz in all samples (Table 1). Clay minerals were detected by XRD in Castlegate, Obernkirchen, and Berea samples, and they are listed as a single mineral group in Table 1. No other minerals except quartz were detected for Bentheimer sandstone samples by XRD and the specific surface measured by the N$_2$ adsorption (the BET method, Brunauer et al., 1938) listed for Bentheimer in Table 1 likewise does not indicate the presence of clay minerals. However,

Figure 3. Model predictions of thermal conductivity from equation 7 as a function of porosity using $\lambda_{\mathrm{lbs}} = 7.7$ Wm^{-1} K^{-1} for quartz (Clauser and Huenges, 1995) and fixed values of $\alpha = 0.7$ and c_M after equation 4. Labels on lines indicate $V_{\mathrm{sus}} = 0.05$, 0.2, and 0.4, respectively. (a) In the dry state, assuming air as saturating fluid and $\lambda_f = 0.024$ Wm^{-1} K^{-1} (Beck, 1976), (b) in the water-saturated state, assuming $\lambda_f = 0.62$ Wm^{-1} K^{-1} equal to that of pure water (Beck, 1976).

backscatter electron micrograph (BSEM) images from sidetrims show the presence of kaolinite suggesting that kaolinite is only locally distributed as clusters within the pore space (Figure 4f). In accordance with Peksa et al. (2017), a clay content of 2.7 mass % is consequently listed for Bentheimer.

Figure 4a–4f shows BSEM images of sidetrims from the studied geologic material. No clay minerals were detected in Fontainebleau samples (Figure 4a–4c). Kaolinite was detected in the Castlegate, Bentheimer, Obernkirchen, and Berea samples (Figure 4d–4h). Figure 4a and 4b shows that weathering of Fontainebleau samples with indices 1 or 2 has led to weak grain contacts. Quartz is the load-bearing mineral in all samples, including the Gassum Formation (GF) sandstone (Figure 4i), which is one formation studied from downhole data.

Experimental methods

Outcrop samples were prepared for laboratory measurement of thermal conductivity in two stages: (1) 75 mm diameter cores were used in the dry state and at atmospheric pressure for measurements of dry thermal conductivity λ_{dry} using an ISOMET 2104 heat-transfer analyzer instrument from Applied Precision Ltd. at an experimental accuracy of 10%, and (2) 38 mm diameter plugs were cored from the larger cores and saturated with demineralized water in vacuum followed by pressurized water submersion. In the saturated state and at atmospheric pressure thermal conductivity, λ_{sat} was measured using a C-Therm TCi instrument from C-THERM TECHNOLOGIES at GFZ, Germany and with 5% accuracy. Applied instruments both use a transient plane source placed directly on sample material to determined thermal conductivity. The sample material was oven dried (60°C) and equilibrated at ambient temperature before measurements of dry density, grain density, and gas-porosity by N_2 expansion, Klinkenberg corrected N_2 permeability, as well as elastic wave velocities. Elastic wave velocities were measured in the dry state with a central frequency of approximately 0.2 MHz for the P-wave V_P, and 0.5 MHz for the S-wave V_s, and at hydrostatic stress σ_h of 40 MPa.

Measured physical parameters of outcrop material

Physical properties measured on outcrop material are shown in Table 2. In accordance with XRD analysis, grain densities close to 2.66 g/cm³ (Table 2) correspond to the dominance of quartz in all outcrop samples (Table 1).

Logging data and core material from ST-18

Downhole data and the corresponding core material used for model validation originate from an exploration well denoted ST-18 and located on mid Zealand near Stenlille, Denmark. The logging campaign conducted on ST-18 included

bulk density, electrical resistivity, natural gamma ray (GR), and P-wave velocity V_P in the depth range from 1250 to 1700 m (Figure 5). The shale interval in ST-18 from 1250 to 1580 m represents the Fjerritslev Formation (FF). Solid volumes of the FF consist of approximately 40% quartz silt, 51% clay minerals dominated by illite and kaolinite and 9% other minerals and with clay being the load-

Table 1. Mineral content from quantitative XRD analysis and specific surface by BET on outcrop material.

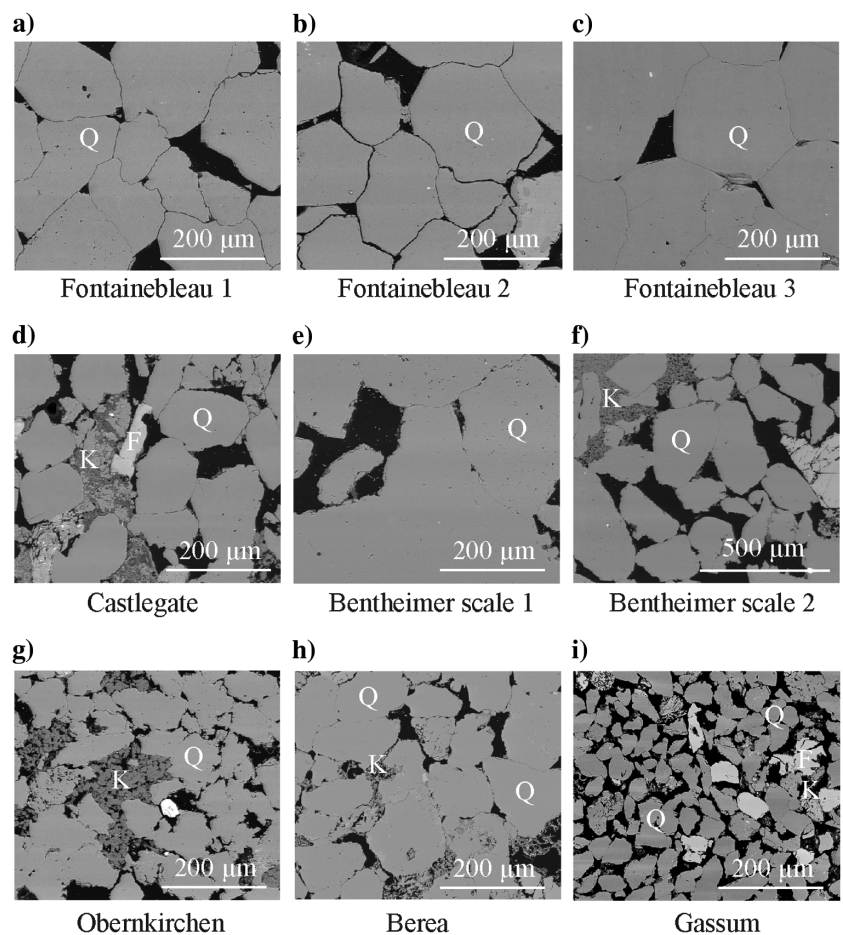| Formation	Quartz	Feldspar	Clay	BET, specific surface
	Mass % of total solid			m²/g
Fontainebleau	100	—	—	0.03
Castlegate	95.4	1.1	3.5	1.72
Bentheimer	95.3	4.7	(2.7)[3]	0.31
Obernkirchen	96.0	—	4.0	1.06
Berea	95.0	—	5.0	1.50

[3]Peksa et al. (2017).

Figure 4. (a-h) BSEM images of polished thin sections from side trims of Fontainebleau, Castlegate, Bentheimer, Obernkirchen, and Berea sandstones. (i) Polished thin section of Gassum sandstone. Q, quartz; F, feldspar; and K, kaolinite.

bearing mineral (Mbia et al., 2014). The interval from 1560 to 1700 m represents the GF and consists of sandstone with a series of clayey interlayered sections. According to Kjøller et al. (2011), the solid volume of the Gassum sandstone is dominated by 85% quartz and small amounts of feldspar and kaolinite (Figure 4i).

Thermal conductivity λ_{amb} was measured on the surface of the slabbed core of ST-18 in an ambient state using the same instrument as for λ_{dry} of outcrop material.

RESULTS

Thermal conductivity of clay constituent

In sandstones, clay minerals often constitute a nonload-bearing mineral and the clay mineral thermal conductivity λ_{clay} would typically represent λ_{sus} as a model input. However, because of the small geometric size of the mineral particles, it is to the authors' best knowledge currently experimentally impossible to measure thermal conductivity of a single clay mineral. In the literature, values of λ_{clay} are given in the range from 1.3 to 3 $\text{Wm}^{-1}\text{K}^{-1}$ (Horai, 1971; Brigaud and Vasseur, 1989; Poelchau et al., 1997), but they represent modeled values typically derived by extrapolating data for porous

clay to zero porosity. Figure 6 shows the experimental results of thermal conductivity for a series of clay samples (Brigaud and Vasseur, 1989). The samples are classified into water-saturated natural clays and recompacted samples of clay mineral powders, which on average contain 93% water and 7% air saturation in the pore space (Brigaud and Vasseur, 1989). Measured thermal conductivity of recompacted samples is hence most likely lower than would be expected for water-saturated samples. For use in the proposed model, we derive an estimated range of λ_{clay} by using the data of recompacted samples from Brigaud and Vasseur (1989). Assuming full water saturation and using the lower Wiener bound in line with the model assumption of nonload-bearing minerals being in suspension with the saturating fluid, we adjust λ_{clay} to enclose the data and thus we deduct the range of λ_{clay} at zero porosity (Figure 6). At zero porosity, the range of λ_{clay} becomes $1.3 - 6.0$ $\text{Wm}^{-1}\text{K}^{-1}$ (Figure 6).

Outcrop material

Bulk and compressional moduli derived from density and ultrasonic velocities (Table 2) are shown in Table 3. Assuming a pure quartz matrix, Biot's coefficients α and δ are derived from equations 1 and 2, respectively, using K_{min} and M_{min} of respectively 37 GPa after

Table 2. Physical properties of the outcrop sample material.

	Grain density	Dry density	Porosity	Permeability	V_P	V_S	TC[9] saturated	TC[9] dry
	ρ_{min}	ρ_{dry}	ϕ	k	$\sigma_h = 40$ MPa		λ_{sat}	λ_{dry}
	cm³/g	cm³/g	–	m²	km/s		$\text{Wm}^{-1}\text{K}^{-1}$	
F1.1[4]	2.66	2.36	0.104	1.34×10^{-13}	5.02	3.30	5.92	2.76
F1.2[4]	2.65	2.46	0.071	1.72×10^{-14}	5.34	3.51	6.08	2.90
F2.1[4]	2.65	2.38	0.084	3.75×10^{-14}	5.20	3.41	5.92	1.81
F2.2[4]	2.66	2.32	0.085	3.86×10^{-14}	5.18	3.45	6.06	2.14
F3.1[4]	2.65	2.52	0.047	6.9×10^{-16}	5.65	3.85	6.32	5.74
F3.2[4]	2.65	2.52	0.046	5.9×10^{-16}	5.67	3.86	6.31	5.75
F3.3[4]	2.65	2.53	0.047	6.9×10^{-16}	5.22	3.56	6.43	5.77
C2.1[5]	2.67	1.91	0.284	3.07×10^{-13}	3.17	2.04	2.75	1.75
C2.2[5]	2.67	1.92	0.279	3.13×10^{-13}	3.44	2.20	2.86	1.88
C2.3[5]	2.67	1.91	0.284	2.84×10^{-13}	3.41	2.15	2.86	1.77
B1[6]	2.67	1.97	0.262	[10]	3.73	2.45	4.71	2.29
B2[6]	2.67	1.98	0.265	[10]	3.16	2.44	4.74	2.29
B3[6]	2.67	1.97	0.263	[10]	3.68	2.84	4.69	2.14
O1[7]	2.67	2.21	0.175	4.86×10^{-13}	4.33	2.84	5.39	3.47
O2[7]	2.67	2.15	0.196	7.30×10^{-13}	4.19	2.76	5.38	3.46
O3[7]	2.67	2.19	0.175	7.30×10^{-13}	4.12	2.75	5.37	3.30
BR1[8]	2.68	2.17	0.190	9.72×10^{-14}	4.00	2.62	4.73	2.46
BR2[8]	2.68	2.20	0.193	1.26×10^{-14}	4.00	2.60	4.74	2.46
BR3[8]	2.68	2.18	0.186	4.64×10^{-14}	4.00	2.60	4.43	2.48

[4]Fontainebleau.
[5]Castlegate.
[6]Bentheimer.
[7]Obernkirchen.
[8]Berea.
[9]Thermal conductivity.
[10]The expected range of the Bentheimer permeability is $4.9 \times 10^{-13} - 2.9 \times 10^{-12}$ m², based on findings of Al-Yaseri et al. (2015) and Peksa et al. (2015).

Carmichael (1961) and 97 GPa using quartz density and P-wave velocity after citations in Mavko et al. (2009) (Table 3).

Crossplots of α and δ from Table 3 show a good linear correlation (Figure 7) with forced zero crossing, and only minor difference is observed. Linear correlation is used in cases in which only the P-wave velocity is available.

A general tendency of increasing thermal conductivity with decreasing porosity is observed for the outcrop samples (Figure 8). All data fall within Wiener bounds and in the dry state also within Hashin-Shtrikman bounds (Figure 8). In the four Fontainebleau samples with first index 1 or 2 and the highest porosity (Table 2), a distinct decrease in thermal conductivity from the saturated to the dry case is observed (Figure 8, circle). The four samples are outliers and fall between the geometric mean and the lower Hashin-Shtrikman bound. The geometric mean approximately captures sample data in the dry and saturated states; however, disregarding outliers, a better fit is found in the dry state in terms of R^2 and root-mean-square (rms) error (Figure 8). To illustrate the effect of α in this work (equation 7), we chose two values of α in Figure 8. In the example, we used (1) c_M after equation 4, (2) quartz as the load-bearing mineral, (3) a nonload-bearing clay volume of $V_{clay} = V_{sus} = 0.05$. For constituents, we assumed thermal conductivities of saturating fluids as in Figure 3, $\lambda_{lbs} = 7.7$ Wm^{-1} K^{-1} for quartz, and $\lambda_{sus} = \lambda_{clay} = 6$ Wm^{-1} K^{-1} for clay in line with the upper value found in Figure 6.

Crossplotting the measured thermal conductivity and Biot's coefficient yields an increasing thermal conductivity for decreasing Biot's coefficient derived at high stress (Figure 9). Fontainebleau samples with the first index 1 or 2 plot as outliers in the dry state (Figure 9a, circle), but not in the saturated state (Figure 9b). Disregarding outliers, trend lines show different slopes for the dry and saturated states, respectively, but in terms of R^2 and rms error, we find good agreement between Biot's coefficient and thermal conductivity using linear correlation (Figure 9). Trend lines cross the y-axis at practically identical values.

Crossplots of modeled (equation 7) and measured thermal conductivity for the outcrop samples are shown in Figure 10. For modeled thermal conductivity, we assumed quartz as the load-bearing mineral and the remaining solids as clays (Table 1; Figure 4). We used (1) values of α from ultrasonic velocities (Table 3), (2) ϕ as listed in Table 2, (3) the clay content listed in Table 1 equal to V_{sus}, (4) thermal conductivities of load-bearing solids and saturating fluids identical to the example in Figure 3, and (5) thermal conductivity of nonload-bearing clay mineral as 6.0 Wm^{-1} K^{-1}. With the exception of the four Fontainebleau samples previously identified as outliers, we find good agreement in terms of rms error between the measured and modeled thermal conductivity in the dry and saturated states (Figure 10).
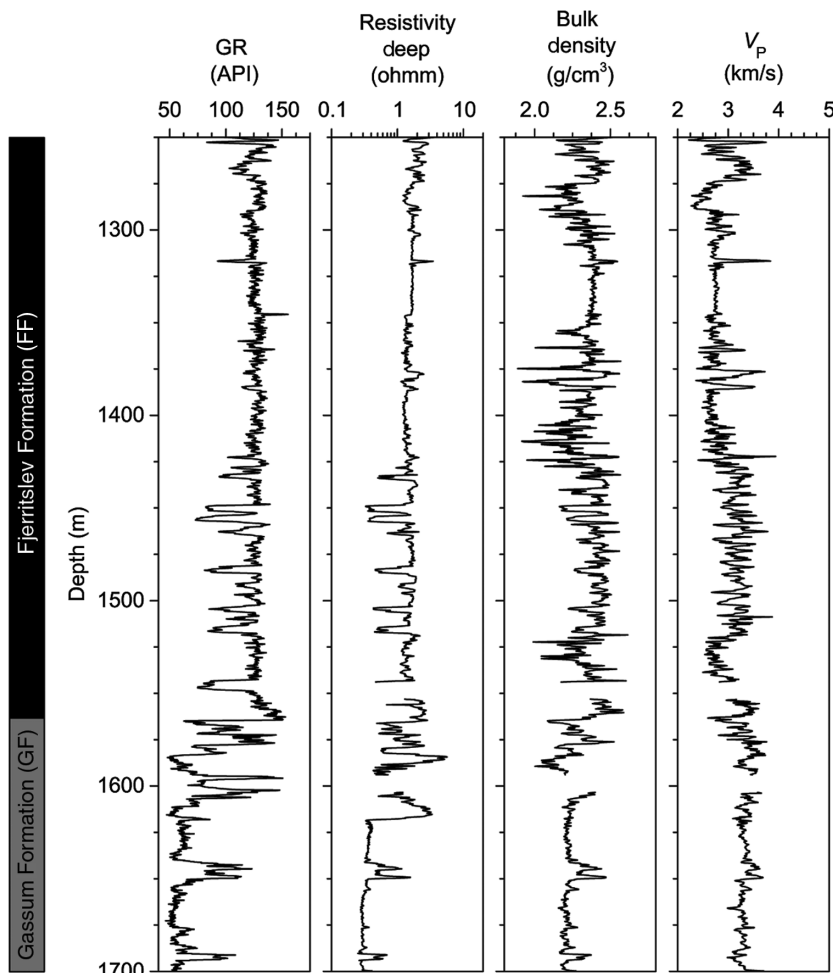

Figure 5. Depth plot from ST-18 of natural GR, electrical resistivity, bulk density, and P-wave velocity V_P.
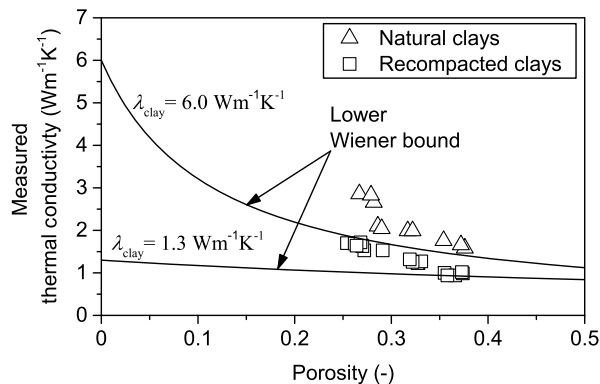

Figure 6. Thermal conductivity versus porosity of recompacted and natural clays. Data are from Brigaud and Vasseur (1989). Lines enclose data of recompacted clay samples by the lower Wiener bound using $\lambda_{clay} = 1.3$ Wm^{-1} K^{-1}, respectively, 6.0 and 0.62 Wm^{-1} K^{-1} as thermal conductivity of water.

Core material from ST-18

Using conventional log interpretation and input from Figure 5, we derived (1) porosity from density and resistivity logs, (2) clay volume V_{clay} with reference to the bulk volume from the GR log as well as porosity, (3) c_M from porosity in accordance with equation 4, and (4) δ from fluid substitution through the approximated Gassmann's equation (Mavko et al., 2009) with the compressional modulus derived from the density and P-wave log and a compressional mineral modulus of 97 GPa as for the outcrop material. The derived parameters are shown in Figure 11a, in which Biot's coefficient α was calculated from δ using the linear correlation from Figure 7 because only P-wave data were logged for ST-18. In general, increasing V_{clay} coincides with decreasing porosity, whereas decreasing porosity coincides with decreasing Biot's coefficient. Biot's coefficient remains close to 0.8.

Table 3. Derived properties of outcrop sample material. The value c is derived by solving equation 3 using the inputs of porosity, permeability (Table 2), and specific surface with respect to the bulk volume calculated from BET (Table 1). The value c_M is calculated from equation 4 using the input of porosity (Table 2).

	Dry bulk modulus K_{dry}	Dry compress. modulus M_{dry}	Biot's coefficient α	δ	Kozeny's factor c	c_M
	$\sigma_h = 40$ MPa		$\sigma_h = 40$ MPa			
	GPa	GPa	–	–	–	–
F1.1[11]	25.12	59.40	0.32	0.39	0.52	0.19
F1.2[11]	29.73	70.08	0.20	0.28	0.22	0.19
F2.1[11]	27.15	64.09	0.27	0.34	0.29	0.19
F2.2[11]	25.40	62.23	0.31	0.36	0.28	0.19
F3.1[11]	30.50	80.43	0.18	0.17	0.03	0.18
F3.2[11]	31.15	81.33	0.16	0.16	0.03	0.18
F3.3[11]	26.27	68.98	0.29	0.29	0.03	0.18
C2.1[12]	8.61	19.17	0.77	0.80	145	0.22
C2.2[12]	10.34	22.72	0.72	0.77	158	0.22
C2.3[12]	10.32	22.12	0.72	0.77	134	0.22
B1[13]	11.66	27.41	0.68	0.72	[16]	0.22
B2[13]	8.20	19.72	0.78	0.80	[16]	0.22
B3[13]	11.09	26.65	0.70	0.73	[16]	0.22
O1[14]	17.65	41.33	0.52	0.57	4.9	0.21
O2[14]	15.30	37.74	0.59	0.61	4.9	0.21
O3[14]	14.81	37.00	0.60	0.62	6.7	0.21
BR1[15]	15.66	35.44	0.58	0.63	148	0.21
BR2[15]	15.74	35.62	0.57	0.63	184	0.21
BR3[15]	15.30	34.97	0.59	0.64	77	0.21

[11]Fontainebleau.
[12]Castlegate.
[13]Bentheimer.
[14]Obernkirchen.
[15]Berea.
[16]The range of c is 10–60 using the expected range of permeability of Table 2.
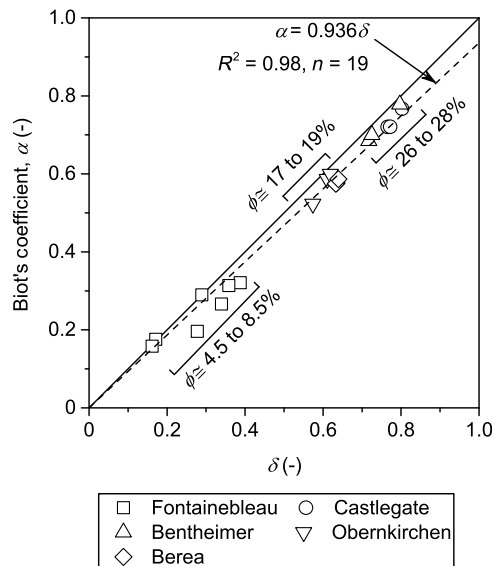

Figure 7. Biot's coefficient α versus δ. Data are from Table 3. The dashed line shows the best linear fit with a forced crossing at zero. The ranges of the sample porosity are shown. The error bars are approximately equal to the marker size.
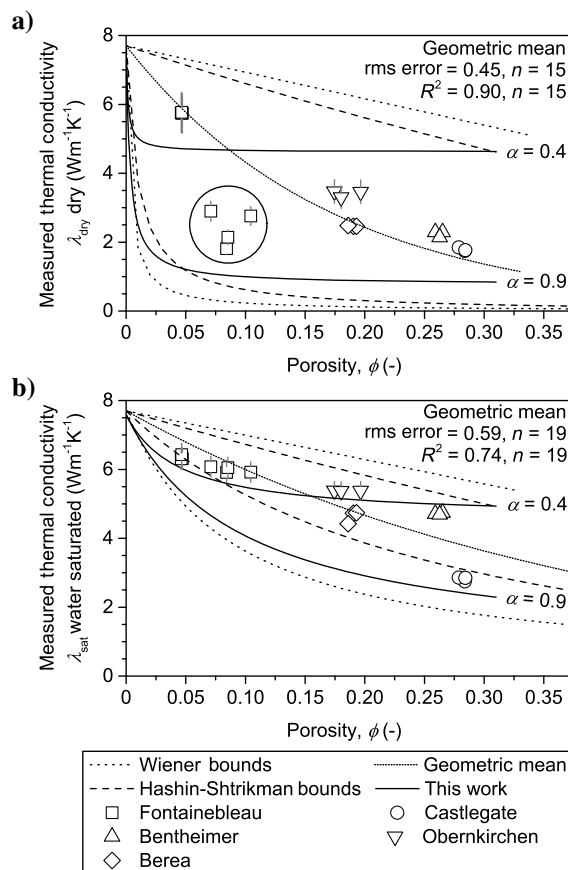

Figure 8. Thermal conductivity versus porosity crossplots of outcrop samples. Outliers (Font., indices 1 and 2) are marked with a circle. Error bars larger than the marker size are shown. (a) In the dry state and (b) in the water-saturated state. Bounds are calculated using the thermal conductivity of quartz equal to 7.7 $Wm^{-1} K^{-1}$ and the values for air and water as in Figure 3.

From equation 7 and by using values from Figure 11a as input, we modeled thermal conductivity as a function of depth for the well ST-18 for the dry and the water-saturated cases (Figure 11b). Based on petrographic evidence (Mbia et al., 2014), we modeled thermal conductivity assuming clay as the load-bearing mineral in sections with $V_{clay}/(1-\phi) > 0.2$. In sections with $V_{clay}/(1-\phi) < 0.2$, we assumed quartz to be load bearing. In general, the depth section from 1250 to 1600 m is identified as clay bearing and the section from 1600 to 1700 m as quartz bearing. In the clay-bearing section, modeled values of thermal conductivity range from 2 to 3 $Wm^{-1}K^{-1}$ in the saturated case (Figure 11b) showing good agreement with experimental results by Brigaud and Vasseur (1989) on natural clays (Figure 6), justifying the use of 6.0 $Wm^{-1}K^{-1}$ as clay thermal conductivity. In the same section, values of dry thermal conductivity range from 0.8 to 2 $Wm^{-1}K^{-1}$ (Figure 11b).

The section from 1600 to 1700 m in Figure 11 is magnified in Figure 12 showing porosity and Biot's coefficient together with modeled results of thermal conductivity from this work, the geometric mean and Hashin-Shtrikman bounds. In the saturated state, model predictions of this work closely approximate the lower

Hashin-Shtrikman bound. However, this is not the case for the dry state (Figure 12b and 12c). In the dry state, the geometric mean, closely approximates model prediction of this work; however, in sections with decreasing porosity and increasing clay volume, the geometric mean overestimates the thermal conductivity compared with measurements (Figure 12b). The available data set does not include thermal conductivity measured at in situ stress conditions, but disregarding the potential stress effect, we find good agreement between modeled and measured thermal conductivities in the dry state, assuming $\lambda_{dry} = \lambda_{amb}$ (Figure 12b). No data of thermal conductivity of saturated samples are available for ST-18.

Data from Figure 12b of thermal conductivity as modeled by, respectively, the geometric mean and this work are plotted versus measured the thermal conductivity (λ_{amb}) in Figure 13. Still assum-
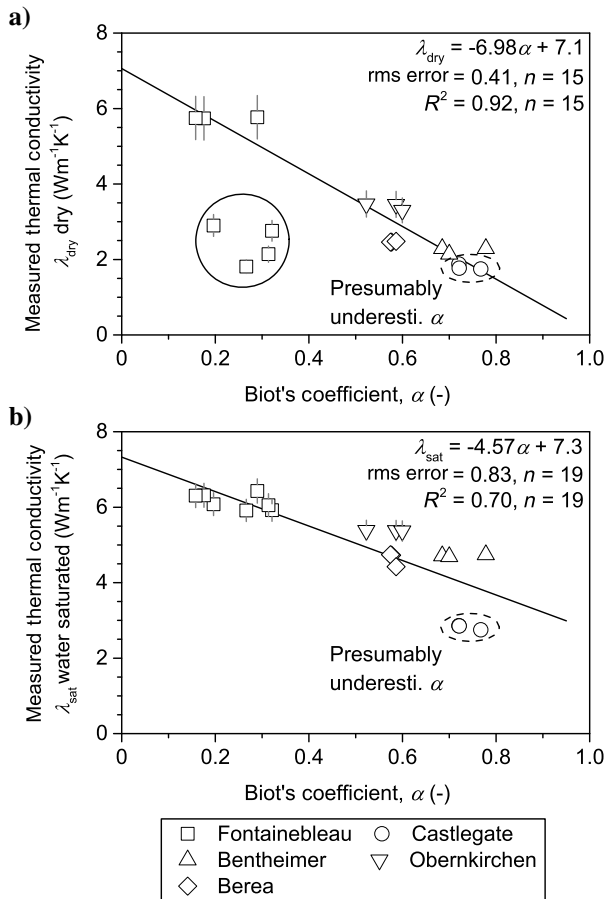

Figure 9. Measured thermal conductivity versus Biot's coefficient crossplots for the samples listed in Tables 2 and 3. Error bars larger than marker size are shown. Outliers are indicated with a circle. The dashed ellipses enclose the Castlegate sample and indicate a presumable underestimation of α because the applied mineral modulus is that of pure quartz, not fully in line with findings from the BSEM images (Figure 4). (a) In the dry state and (b) in the water-saturated state.
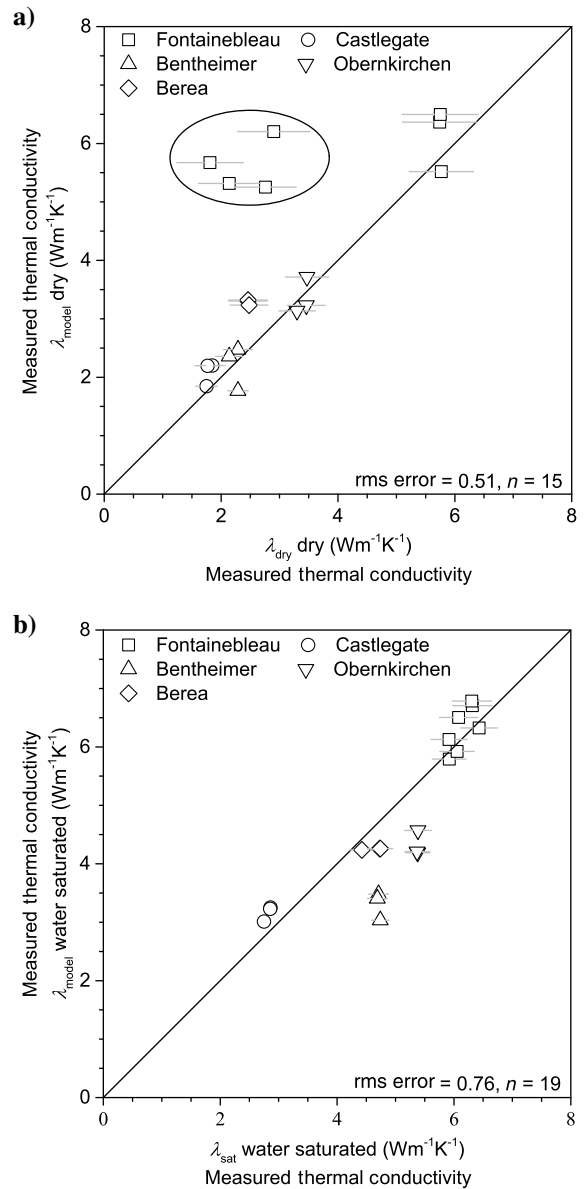

Figure 10. Modeled thermal conductivity (equation 7) versus measured thermal conductivity. Error bars larger than the marker size are shown. (a) In the dry state and (b) in the water-saturated state.

ing $\lambda_{dry} = \lambda_{amb}$, the geometric mean shows a larger scatter and derived rms error values illustrate a better fit for this work.

DISCUSSION

Any given model designed for prediction of downhole thermal conductivity and based on logging data must be theoretically based to secure application beyond the constraints of empirical relations. Furthermore, it should be judged by its ability to predict within sufficient accuracy, independent of saturating fluid and mineralogy of the solid constituents.

Our data show that the texture found in sandstones cannot completely be captured in the dry and water-saturated cases by use of conventional two-constituent porosity-based models (Figure 8); however, the geometric mean provides a good approximation. Further, the data show decreasing thermal conductivity for increasing Biot's coefficient illustrating a significant contribution of heat transfer through the solid, but as the general trends are different for air and water, the contributions from the saturating fluid are significant (Figure 9). Four of the studied Fontainebleau samples deviated distinctly in crossplots both of thermal conductivity with porosity and

Biot's coefficient (Figures 8 and 9). It is, however, only in the dry state, which illustrates an influence of saturating fluid on the solid heat transfer, when grain contacts are weak or nonexisting (Figure 4a and 4b) causing insufficient surface contact between the sample material and the measuring sensor. When quantifying regressions and model predictions, we disregard outliers in the dry case, but not for saturated samples. The discrepancy in counted samples (n) does, however, not change the outcome because saturated values of thermal conductivity measured on Fontainebleau samples range within 0.5 Wm^{-1} K^{-1}.

For outcrop specimens, we derived Biot's coefficient at a hydrostatic stress level of 40 MPa corresponding to a presumable maximum contact area between grain contacts, and with the exception of the mentioned Fontainebleau samples in the dry state, we observed good agreement with the experimental results, and compared with the geometric mean, differences in the rms error are minor (Figures 8 and 10). This indicates that at the applied boundary conditions, the solid heat transfer cross section is equal to that of the grain contacts (Figure 10). This justifies the applicability of using material stiffness for prediction of thermal conductivity as was proposed by, e.g., Horai and Simmons (1969), Zamora et al. (1993), Kazatchenko et al.
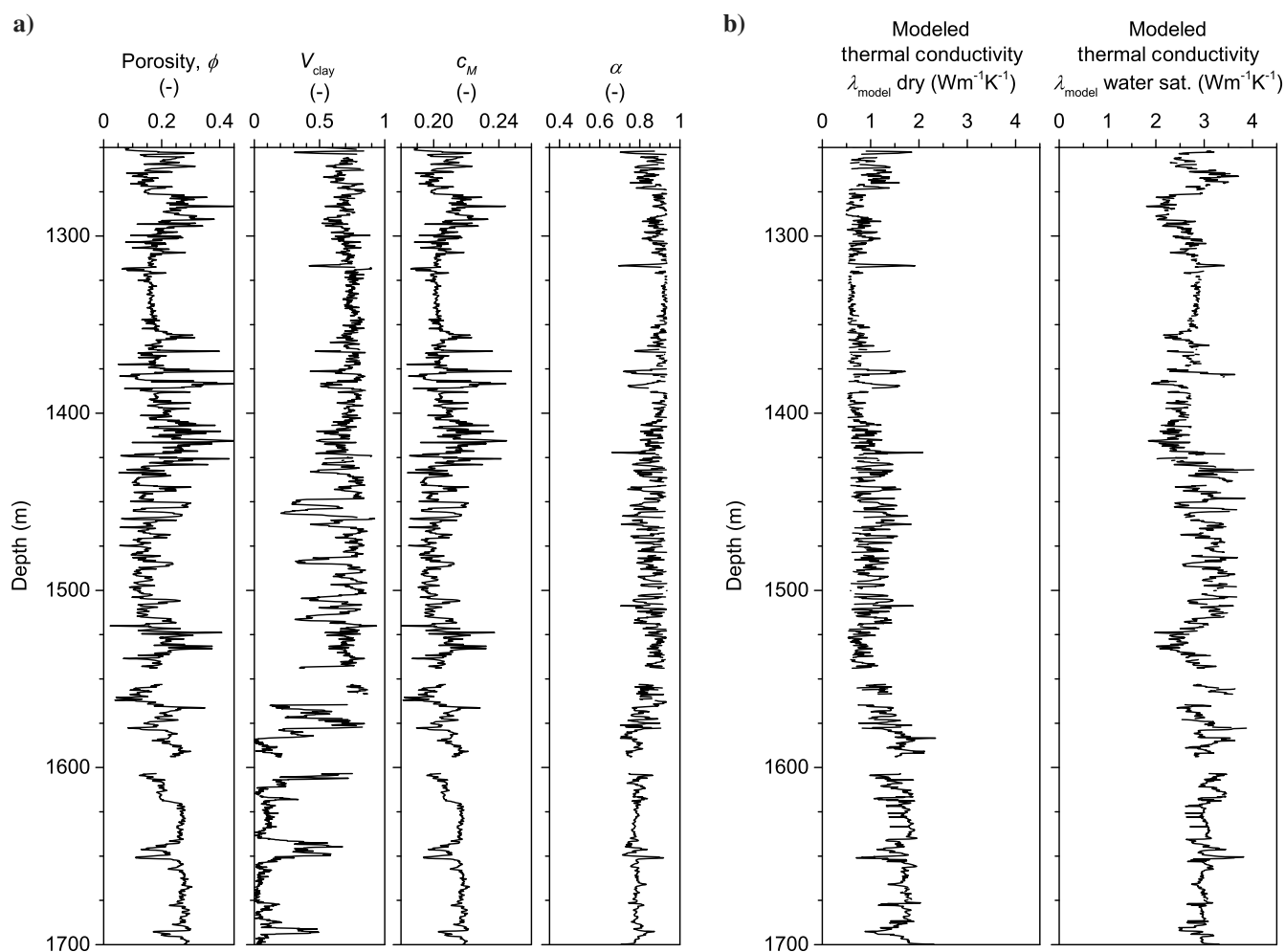

Figure 11. (a) Depth plot of derived porosity, clay volume (V_{clay}), c_M and Biot's coefficient (α). (b) Modeled thermal conductivity in the dry and saturated states of well ST-18 as a function of depth using input from Figure 11a, λ_{clay} of 6 Wm^{-1} K^{-1} and additional constituent thermal conductivities as in Figure 2.

(2006), Gegenhuber and Schoen (2012), and Pimienta et al. (2014), but with the use of empirical relations or empirical parameters. The weak grain contacts found in outliers of Fontainebleau samples (Figures 8a, 9a, and 10), illustrate the discrepancy between the boundary conditions at which the thermal conductivity is measured, respectively, modeled. The discrepancy causes an overestimation of the physical solid heat transfer controlled by the weak grain contacts when the thermal conductivity is modeled from Biot's coefficient and thereby maximum closure of the grain contacts. Our data set does not include the possibility for quantification of discrepancies in the boundary conditions between the input for the modeled and the measured thermal conductivities because the latter was only measured at ambient conditions. However, Horai and Susaki (1989) and Abdulagatova et al. (2009) show an order of 0.1 $Wm^{-1}K^{-1}$ increase in thermal conductivity following a 40 MPa stress increase for sandstones with intact grain contacts. In contrast, Lin et al. (2011) show an increase in the order of $1-2$ $Wm^{-1}K^{-1}$ for Rajasthan sandstone, Japan, Shirahama sandstone, India, and Berea sandstone, USA, in the approximate stress range, but with a dependency of the saturating fluid. In general, the presumable increase in thermal conductivity due to stress is not believed to change the finding that the solid heat transfer cross section is equal to the cross section governing the solid stiffness in cases in which weathering or tensile stress-induced microcracks is limited (Figure 10).
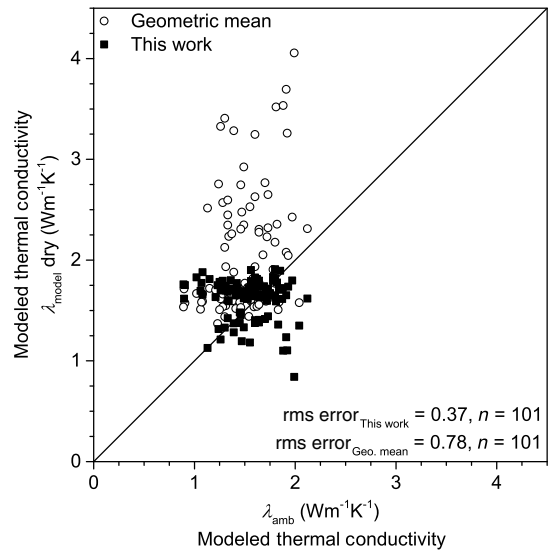

Figure 13. Measured thermal conductivty versus modeled thermal conductivity. The round and square markers show the modeled results of, respectively, the geometric mean and this work. Data are from Figure 12b.
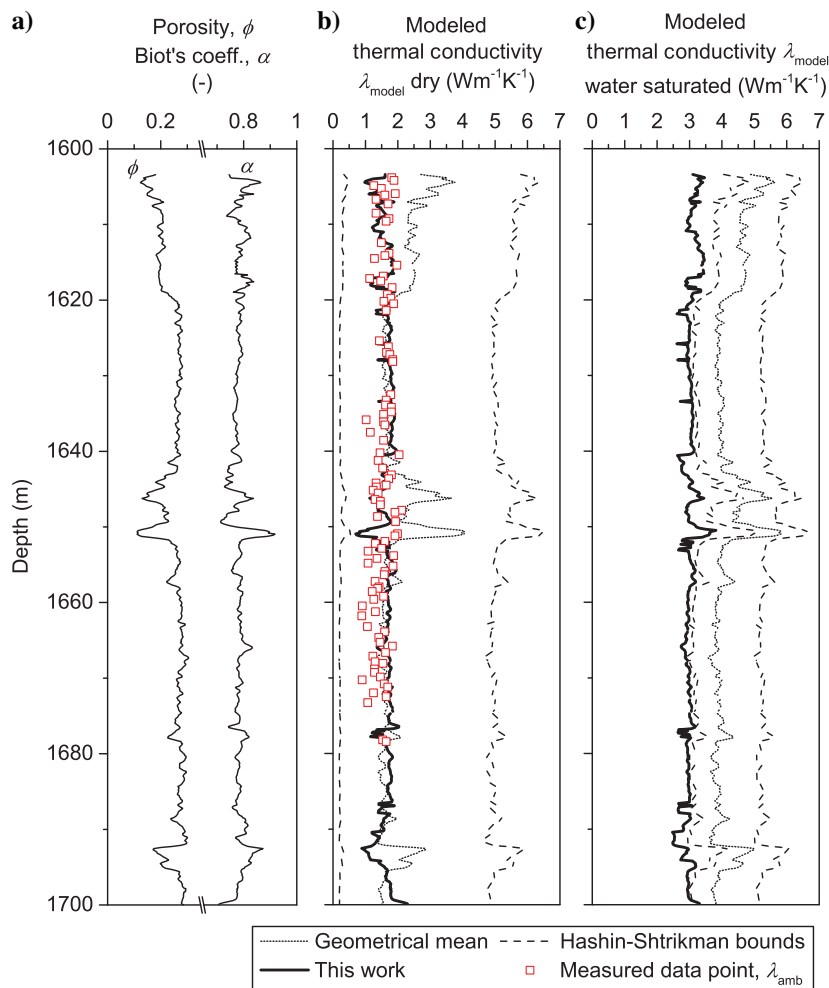

Figure 12. Depth plots of section from 1600 to 1700 m showing porosity, Biot's coefficient, and modeled thermal conductivities from geometric mean, the Hashin-Shtrikman bounds, and this work. (a) In situ porosity and Biot's coefficient. (b) In the dry state, further with laboratory measured data points at ambient conditions. (c) In the water-saturated state.

The heterogeneity in distribution of specific surface in the studied sandstones containing clay is illustrated by the range of derived values for Kozeny's factor c. No effect of specific surface is included in the proposed model, but only shielding effects obstructing direct heat transfer in the pore space. This emphasizes the importance of using c_M in the modeling of thermal conductivity and not Kozeny's factor c.

Predictions of thermal conductivity from logging data of the investigated shale formation range within experimental values found in the literature, justifying the use of clay thermal conductivity two to four times those published elsewhere (e.g., Horai, 1971; Brigaud and Vasseur, 1989; Poelchau et al., 1997) (Figures 3, 6, and 11b). Further, in the studied sandstone formation, we see a good agreement between modeled and measured thermal conductivity (Figure 12) justifying the proposed model and its applicability in downhole logging also in cases with a lack of S-wave data, such as the present because the correction from δ to α is minor (Figure 7). Compared with the geometric mean, the proposed model provides more accurate estimates of thermal conductivity in general (Figures 12 and 13), but, especially in the clayey sandstone sections with low porosity (Figure 12a and 12b), our model provides a good agreement with experimental results, further justifying the applied value of clay thermal conductivity.

CONCLUSION

We used laboratory and logging data to validate a theoretical model of thermal conductivity with application to sandstones. The proposed model includes quantifications of solid and fluid heat transfer cross sections derived from measurable parameters, and it is able to predict thermal conductivity with good agreement to experimental results using either laboratory or logging data as input, hence showing an improvement compared with porosity-based models. Further, because input data are derived from well-known physical properties, constraints of locality, implicit when using empirical relations, are removed. The model is able to address mixed mineralogy provided that the detailed mineralogy is known but it is, however, limited to a single load-bearing mineral. The obtained results showed that with closure of open grain contacts by stress increase, heat transfer through the solids can be estimated through Biot's coefficient.

ACKNOWLEDGMENTS

APPENDIX A

FORMULATION OF GEOMETRIC MEAN, WIENER BOUNDS, AND HASHIN-SHTRIKMAN BOUNDS

In this appendix, we summarize formulations of the geometric mean, Wiener bounds, and Hashin-Shtrikman bounds because the proposed model is compared with these. For a two-constituent mixture, the geometric mean is formulated as

$$\lambda_{\text{geo}} = \lambda_f^{\phi} \lambda_s^{1-\phi}, \qquad (A\text{-}1)$$

where ϕ, λ_f, and λ_s are the porosity and thermal conductivity of, respectively, the fluid and solid constituent.

In accordance with Wiener (1904), the Wiener bounds are for a two-constituent mixture formulated as

$$\lambda_{W,l} = \left(\frac{\phi}{\lambda_f} + \frac{1-\phi}{\lambda_s} \right)^{-1} \text{ (lower bound)}, \qquad (A\text{-}2)$$

$$\lambda_{W,u} = \phi \lambda_f + (1-\phi)\lambda_s \text{ (upper bound)}, \qquad (A\text{-}3)$$

where ϕ, λ_f, and λ_s are the porosity and thermal conductivity of, respectively, the fluid and solid constituent.

In accordance with Hashin and Shtrikman (1962), the lower and upper Hashin-Shtrikman bounds are for a isotropic and homogeneous two-constituent mixture with $\lambda_s < \lambda_f$ formulated as

$$\lambda_{\text{HS},l} = \lambda_f + \frac{1-\phi}{\frac{1}{\lambda_s - \lambda_f} + \frac{\phi}{3\lambda_f}} \text{ (lower bound)}, \qquad (A\text{-}4)$$

$$\lambda_{\text{HS},u} = \lambda_s + \frac{\phi}{\frac{1}{\lambda_f - \lambda_s} + \frac{1-\phi}{3\lambda_s}} \text{ (upper bound)}, \qquad (A\text{-}5)$$

where ϕ, λ_f, and λ_s are the porosity and the thermal conductivity of, respectively, the fluid and solid constituent.

REFERENCES

Abdulagatova, Z., I. M. Abdulagatov, and V. N. Emirov, 2009, Effect of temperature and pressure on the thermal conductivity of sandstone: International Journal of Rock Mechanics and Mining Sciences, **46**, 1055–1071, doi: 10.1016/j.ijrmms.2009.04.011.

Alam, M. M., I. L. Fabricius, and H. F. Christensen, 2012, Static and dynamic effective stress coefficient of chalk: Geophysics, **77**, no. 2, L1–L11, doi: 10.1190/geo2010-0414.1.

Al-Yaseri, A. Z., M. Lebedev, S. J. Vogt, M. L. Johns, A. Barifcani, and S. Iglauer, 2015, Pore-scale analysis of formation damage in Bentheimer sandstone with in-situ NMR and micro-computed tomography experiments: Journal of Petroleum Science and Engineering, **129**, 48–57, doi: 10.1016/j.petrol.2015.01.018.

Batchelor, G. K., and R. W. O'Brien, 1977, Thermal or electrical conduction through a granular material: Proceedings of the Royal Society of London: Series, A, **355**, 313–333, doi: 10.1098/rspa.1977.0100.

Beck, A. E., 1976, An improved method of computing the thermal conductivity of fluid-filled sedimentary rocks: Geophysics, **41**, 133–144, doi: 10.1190/1.1440596.

Biot, M. A., 1941, General theory for three-dimensional consolidation: Journal of Applied Physics, **12**, 155–164, doi: 10.1063/1.1712886.

Brigaud, F., and G. Vasseur, 1989, Mineralogy, porosity and fluid control on thermal conductivity of sedimentary rocks: Geophysical Journal, **98**, 525–542, doi: 10.1111/j.1365-246X.1989.tb02287.x.

Brunauer, S., P. H. Emmett, and E. Teller, 1938, Adsorption of gases in multimolecular layers: Journal of the American Chemical Society, **60**, 309–319, doi: 10.1021/ja01269a023.

Carmichael, R. S., 1961, Practical handbook of physical properties of rocks and minerals: CRC Press.

Clauser, C., and E. Huenges, 1995, Thermal conductivity of rocks and minerals, *in* T. J. Ahrens, ed., Rock physics and phase relations: A handbook of physical constants: American Geophysical Union, 105–126.

Deissler, R. D., and C. S. Eian, 1952, Investigation of effective thermal conductivity of powders: Technical report NACA RM E52C05, National Advisory Committee for Aeronautics.

Fabricius, I. L., 2010, A mechanism for water weakening of elastic moduli and mechanical strength of chalk: 80th Annual International Meeting, SEG, Expanded Abstracts, 2736–2740.

Freifeld, B. M., S. Finsterle, T. C. Onstott, P. Toole, and L. M. Pratt, 2008, Ground surface temperature reconstructions: Using in situ estimates for thermal conductivity acquired with a fiber-optic distributed thermal perturbation sensor: Geophysical Research Letters, **35**, L14309, doi: 10.1029/2008GL034762.

Fuchs, S., and A. Förster, 2014, Well-log based prediction of thermal conductivity of sedimentary successions: A case study from the North German Basin: Geophysical Journal International, **196**, 291–311, doi: 10.1093/gji/ggt382.

Gassmann, F., 1951, Über die elastizität poröser medien: Veirteljahrsschrift der Naturforschenden Gesellschaft in Zürich, **96**, 1–23.

Gegenhuber, N., and J. Schoen, 2012, New approaches for the relationship between compressional wave velocity and thermal conductivity: Journal of Applied Geophysics, **76**, 50–55, doi: 10.1016/j.jappgeo.2011.10.005.

Gommesen, L., I. L. Fabricius, T. Mukerji, G. Mavko, and J. M. Pedersen, 2007, Elastic behavior of North Sea chalk: A well-log study: Geophysical Prospecting, **55**, 307–322, doi: 10.1111/j.1365-2478.2007.00622.x.

Hadley, G. R., 1986, Thermal conductivity of packed metal powders: International Journal of Heat Mass Transfer, **29**, 909–920, doi: 10.1016/0017-9310(86)90186-9.

Hartmann, A., V. Rath, and C. Clauser, 2005, Thermal conductivity from core and well log data: International Journal of Rock Mechanics and Mining Science, **42**, 1042–1055, doi: 10.1016/j.ijrmms.2005.05.015.

Hashin, Z., and S. Shtrikman, 1962, A variational approach to the theory of the effective magnetic permeability of multiphase materials: Journal of Applied Physics, **33**, 3125–3131, doi: 10.1063/1.1728579.

Horai, K., 1971, Thermal conductivity of rock-forming minerals: Journal of Geophysical Research, **76**, 1278–1308, doi: 10.1029/JB076i005p01278.

Horai, K., and G. Simmons, 1969, Thermal conductivity of rock-forming minerals: Earth and Planetary Science Letters, **6**, 359–368, doi: 10.1016/0012-821X(69)90186-1.

Horai, K., and J. Susaki, 1989, The effect of pressure on the thermal conductivity of silicate rocks up to 12 kbar: Physics of the Earth and Planetary Interiors, **55**, 292–305, doi: 10.1016/0031-9201(89)90077-0.

Hsu, C. T., P. Cheng, and K. W. Wong, 1994, Modified Zehner-Schlunder models for stagnant thermal conductivity of porous media: International Journal of Heat Mass Transfer, **37**, 2751–2759, doi: 10.1016/0017-9310(94)90392-1.

Huang, J. H., 1971, Effective thermal conductivity of porous rocks: Journal of Geophysical Research, **76**, 6420–6427, doi: 10.1029/JB076i026p06420.

Kazatchenko, E., M. Markov, and A. Mousatov, 2006, Simulation of acoustic velocities, electrical and thermal conductivities using unified pore-structure model of double-porosity carbonate rocks: Journal of Applied Geophysics, **59**, 16–35, doi: 10.1016/j.jappgeo.2005.05.011.

Kjøller, C., R. Weibel, K. Bateman, T. Laier, L. H. Nielsen, P. Frykman, and N. Springer, 2011, Geochemical impacts of CO₂ storage in saline aquifers with various mineralogy: Results from laboratory experiments and reactive geochemical modeling: Energy Procedia, **4**, 4724–4731, doi: 10.1016/j.egypro.2011.02.435.

Kozeny, J., 1927, Über kapillare Leitung des Wassers im Boden: Sitzungsberichte der Wiener Akademie der Wissenschaften, **136**, 271–306.

Kunii, D., and J. M. Smith, 1959, Heat transfer characteristics of porous rocks: AIChE Journal, **6**, 71–78, doi: 10.1002/aic.690060115.

Lin, W., O. Tadai, T. Hirose, W. Tanikawa, M. Takahashi, H. Mukoyoshi, and M. Kinoshita, 2011, Thermal conductivities under high pressure in core samples from IODP NanTroSEIZE drilling site C0001: Geochemistry Geophyics Geosystems, **12**, Q0AD14, doi: 10.1029/2010GC003449.

Mavko, G., T. Mukerji, and J. Dvorkin, 2009, The rock physics handbook, 2nd ed.: Cambridge U.P.

Mbia, E. N., I. L. Fabricius, A. Krogsbøll, P. Frykman, and F. Dalhoff, 2014, Permeability, compressibility and porosity of Jurassic shale from the Norwegian-Danish Basin: Petroleum Geoscience, **20**, 257–281, doi: 10.1144/petgeo2013-035.

Midttomme, K., and E. Roaldset, 1998, The effect of grain size on thermal conductivity of quartz sands and silts: Petroleum Geoscience, **4**, 165–172, doi: 10.1144/petgeo.4.2.165.

Mortensen, J., F. Engstrøm, and I. Lind, 1998, The relation among porosity, permeability, and the specific surface of chalk from the Gorm field, Danish North Sea: SPE Reservoir Evaluation and Engineering, **1**, 245–251, doi: 10.2118/31062-PA.

Moscoso Lembcke, L. G., D. Roubinet, F. Gidel, J. Irvin, P. Pehme, and B. L. Parker, 2016, Analytical analysis of borehole experiments for the estimation of subsurface thermal properties: Advances in Water Resources, **91**, 88–103, doi: 10.1016/j.advwatres.2016.02.011.

Peksa, A. E., K.-H. A. A. Wolf, E. C. Slob, Ł. Chmura, and P. L. J. Zitha, 2017, Original and pyrometamorphical altered Bentheimer sandstone: Petrophysical properties, surface and dielectric behavior: Journal of Petroleum Science and Engineering, **149**, 270–280, doi: 10.1016/j.petrol.2016.10.024.

Peksa, A. E., K-H. A. A. Wolf, and P. L. J. Zitha, 2015, Bentheimer sandstone revisited for experimental purposes: Marine and Petroleum Geology, **67**, 701–719, doi: 10.1016/j.marpetgeo.2015.06.001.

Pimienta, L., J. Sarout, L. Esteban, and C. Delle Piane, 2014, Prediction of rocks thermal conductivity from elastic wave velocities mineralogy and microstructure: Geophysical Journal International, **197**, 860–874, doi: 10.1093/gji/ggu034.

Poelchau, H. S., D. R. Baker, T. Hantschel, B. Horsfield, and B. P. Wygrala, 1997, Basin simulation and design of the conceptual basin model, *in* D. H. Welte, B. Horsfield, and D. R. Baker, eds., Petroleum and basin evolution: Springer-Verlag, 5–70.

Revil, A., 2000, Thermal conductivity of unconsolidated sediments with geophysical applications: Journal of Geophysical Research Letter, **105**, 16.749–16.768, doi: 10.1029/2000JB900043.

Sass, J. H., A. H. Lachenbruch, and R. J. Munroe, 1971, Thermal conductivity of rocks from measurements of fragments and its application to heat-flow determination: Journal of Geophysical Research, **76**, 3391–3401, doi: 10.1029/JB076i014p03391.

Tarnawski, V. R., and W. H. Leong, 2012, A series-parallel model for estimating the thermal conductivity of unsaturated soils: International Journal of Thermophysics, **33**, 1191–1218, doi: 10.1007/s10765-012-1282-1.

Tong, F., L. Jing, and R. W. Zimmerman, 2009, An effective thermal conductivity model of geological porous media for coupled thermos-hydro-mechanical systems with a multiphase flow: International Journal of Rock Mechanics and Mining Sciences, **46**, 1358–1369, doi: 10.1016/j.ijrmms.2009.04.010.

Troschke, B., and H. Burkhardt, 1998, Thermal conductivity models for two-phase systems: Physics and Chemistry of the Earth, **23**, 351–355, doi: 10.1016/S0079-1946(98)00036-6.

Wiener, O., 1904, Lamellare Doppelbrechung: Zeitschrift für Physik, **5**, 332–338.

Woodside, W., and J. H. Messmer, 1961a, Thermal conductivity of porous media. I: Unconsolidated sands: Journal of Applied Physics, **32**, 1688–1699, doi: 10.1063/1.1728419.

Woodside, W., and J. H. Messmer, 1961b, Thermal conductivity of porous media. II: Consolidated rocks: Journal of Applied Physics, **32**, 1699–1706, doi: 10.1063/1.1728420.

Zamora, M., D. Vo-Thanh, G. Bienfait, and J. P. Poirier, 1993, An empirical relationship between thermal conductivity and elastic wave velocities in sandstone: Geophysical Research Letters, **20**, 1679–1682, doi: 10.1029/92GL02460.

Zimmerman, R. W., 1989, Thermal conductivity of fluid-saturated rocks: Journal of Petroleum Science and Engineering, **3**, 219–227, doi: 10.1016/0920-4105(89)90019-3.